Computers and Structures 220 (2019) 1–13

Contents lists available at ScienceDirect

Computers and Structures

journal homepage: www.elsevier.com/locate/compstruc

On the finite element modeling of COPVs

Juan Pablo Canal [1], Alejandro Micuzzi [2], Hernán Logarzo [3], Ariel Terlisky, Rita Toscano, Eduardo Dvorkin *

SIM&TEC S.A., Av. Pueyrredón 2130, C1119ACR Ciudad de Buenos Aires, Argentina

ARTICLE INFO

Article history:
Received 13 February 2019
Accepted 19 April 2019

ABSTRACT

In this paper we discuss the finite element modeling of Composite Overwrapped Pressure Vessels (COPVs) which are used in the aerospace industry, when high *strength/weight* ratios are required, for containers filled with pressurized fluids. The COPVs that we analyze are composed by a thin metallic liner and an external reinforcement made with high strength fibers that are wrapped around the liner embedded in an epoxy resin. It is shown in the paper that for a reliable description of the vessels behavior under internal pressure it is required to use a model that incorporates the mechanical behavior of the liner, of the fibers and of the resin matrix (micromechanical model).

1. Introduction

The modern trend for the construction of pressure vessels with very high *strength/weight* ratio is to use **Composite Overwrapped Pressure Vessels** (COPVs). These pressure vessels, mostly used in the aerospace industry, are constructed using a very thin metallic or non-metallic liner that provides sealability for the contained pressurized fluid, and an external reinforcement composed by high strength fibers (e.g. carbon fibers) that provides the required vessel strength.

During a vessel fabrication, several fiber plies are used, each of them with a defined winding angle. The fibers in each ply are coiled embedded in a resin and the complete assembly is cured in a convection furnace to get the matrix final mechanical properties.

A thorough description of the fibers winding geometry and strength of the resulting laminated shell was provided by Vasiliev in [1]. A number of regulation agencies have produced standards for the design and construction of COPVs, for example the American Institute of Aeronautics and Astronautics (AIAA) [2] and the European Cooperation for Space standardization (ECSS) [3].

In the present paper we discuss the finite element modeling of the COPVs.

In the second section, following the work of Vasiliev, we present a summary of the fiber plies geometry for cylindrical vessels with ellipsoidal heads and for spherical vessels. In the third section we present two alternatives for simulating, using finite element models, the COPVs fibers reinforcement,

- a standard elastic - orthotropic material model; with material properties that average the properties of the fibers and of the matrix;
- a micromechanical material model for each ply, with a proper modeling of the fibers behavior using an elastic - orthotropic model and of the matrix behavior using an anisotropic – plastic model to simulate the loss of stiffness due to the matrix cracking [1].

Both material models were developed with the general purpose finite element code ADINA [4] using its quadrilateral shell element [5]. In the fourth section of this paper we discuss the computational results obtained when modeling,

- a split ring test, which is the lab test used to characterize the strength of a fiber laminate;
- a cylindrical vessel with ellipsoidal heads under internal pressure.

For both cases we compare the numerical results with experimental results to cross validate the model and the manufacturing procedures.

We demonstrate that the new micromechanical model very much improves the results that are obtained using the standard elastic - orthotropic material model.

* Corresponding author.
E-mail address: edvorkin@simytec.com (E. Dvorkin).
[1] Now at INVAP, Bariloche, Argentina.
[2] Now independent consultant, Argentina.
[3] Now at Georgia Tech, Atlanta, GA, USA.

https://doi.org/10.1016/j.compstruc.2019.04.007
0045-7949/

2. Winding geometry

Each laminate is fabricated by coiling carbon fibers, embedded in an epoxy resin, around an aluminum liner. In this section we discuss the geometry of the laminate following [1].

We draw the meridian of a shell of revolution and in what follows we will use the following normalized notation (see Fig. 1),

$$\sin\alpha = -\frac{dz}{ds};\quad \bar{r} = \frac{r}{R};\quad \bar{z} = \frac{z}{R};\quad \bar{z}' = \frac{d\bar{z}}{d\bar{r}}$$

We consider a general fibrous shell of revolution with fibers following trajectories with angles $\varphi(r)$ with the meridians, as shown in Fig. 2.

The equilibrium of the fibers, shown in Fig. 2, is determined neglecting the contribution of the liner and using (*netting analysis*) [1],

$$p\ \pi\ r^2 = n\ t \sin\alpha(r)\cos\varphi(r). \tag{1}$$

In the above equation p is the pressure inside the vessel, t is the tension in the fibers and n is the number of fibers in the shell cross section.

The fiber trajectories are defined by the Clairaut equation (geodesic lines),

$$\bar{r}\ \sin\varphi\left(\bar{r}\right) = \sin\varphi(R). \tag{2}$$

The equations that define the shell meridian for the ellipsoidal shell are [1],

$$\bar{z} = -\int_1^{\bar{r}} \frac{s^3}{\sqrt{(1-s^2)\left(s^2-\bar{r}_1^{-2}\right)\left(s^2+\bar{r}_2^{-2}\right)}}ds \tag{3.a}$$

$$\bar{r}_{1,2}^{-2} = \frac{1}{2}\left(\sqrt{1+4\tan^2\varphi_R}\mp 1\right). \tag{3.b}$$

The above equations are only valid for $0 \le \varphi(R) < \varphi_o$ where, $\varphi_o = 0$, corresponds to a shell with fibers along its meridians. φ_o = 54.7356°, the equation degenerates into a circular cylindrical shell [1].

At the polar hole of the vessel there is usually a fitting, as shown in Fig. 3; the radius $r_f = 1.225 r_o$, indicated in the figure, corresponds to the meridian inflection point [1].

Winding a fibrous band of width w and thickness δ placed on a surface of revolution specified by the equation $z = z(r)$ produces a fibrous shell with a thickness defined by,

$$h(r) = \frac{n\ \delta\ w}{2\ \pi\ r\ \cos\varphi(r)}. \tag{4.a}$$

which can be rewritten as,

$$h(r) = h(R)\frac{R\ \cos\varphi(R)}{r\ \cos\varphi(r)}. \tag{4.b}$$

It is immediate that the above equation fails in the neighborhood of the polar hole ($r = r_o$) because, $\lim_{\varphi(r)\to\pi/2} h(r) = \infty$.

Calling $\bar{h} = \frac{h}{h(R)}$ in the neighborhood of the polar hole the thickness is approximated using,

$$\bar{h}_a\left(\bar{r}\right) = a_o + a_1\bar{r} + a_2\bar{r}^2 + a_3\bar{r}^3. \tag{5}$$

The parameters of the polynomial expansion are determined using the following four conditions,

1. For $\bar{r} = \bar{r}_o$, it is used either $\bar{h}_a\left(\bar{r}_o\right) = 2$or experimental values if they are available;
2. Defining $\bar{r}_{2w} = \bar{r}_o + \frac{2w}{R}$, the continuity between the two thickness definitions is, $\bar{h}_a\left(\bar{r}_{2w}\right) = \bar{h}\left(\bar{r}_{2w}\right)$;

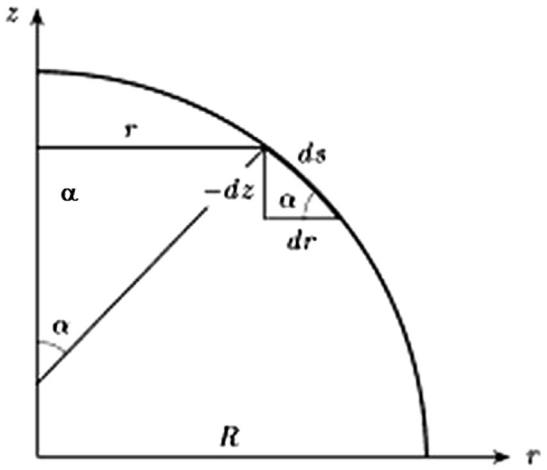

Fig. 1. Meridian of a shell of revolution [1].

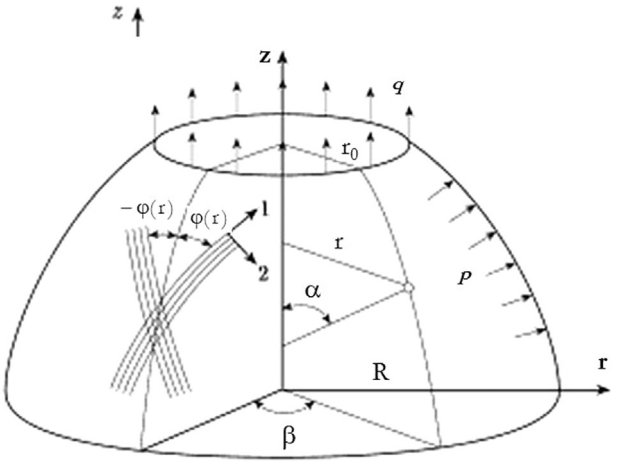

Fig. 2. Isotensoidal shell of revolution [1].

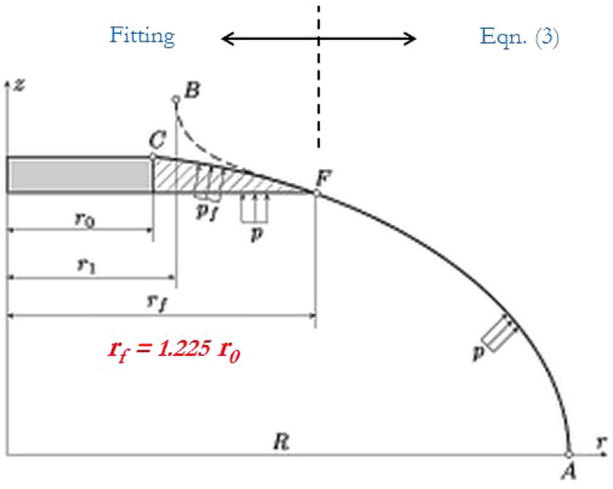

Fig. 3. Fitting at the vessel polar hole [1].

3. The slope continuity is, $\left[\frac{d\bar{h}_a(\bar{r})}{d\bar{r}}\right]_{\bar{r}_{2w}} = \left[\frac{d\bar{h}(\bar{r})}{d\bar{r}}\right]_{\bar{r}_{2w}}$;
4. The mass equivalency is: $\int_{\bar{r}_o}^{\bar{r}_{2w}} \bar{h}_a(\bar{r})d\bar{r} = \int_{\bar{r}_o}^{\bar{r}_{2w}} \bar{h}(\bar{r})d\bar{r}$.

In Fig. 4 we present a graph of the resulting laminate thickness distribution for a 600 mm spherical COPV.

Finally, in Figs. 5 and 6 we present photographs of the winding process implemented at an Argentinian company. In the first case the photograph corresponds to the fabrication of a cylindrical shell with ellipsoidal heads and in the second case to the fabrication of a spherical shell.

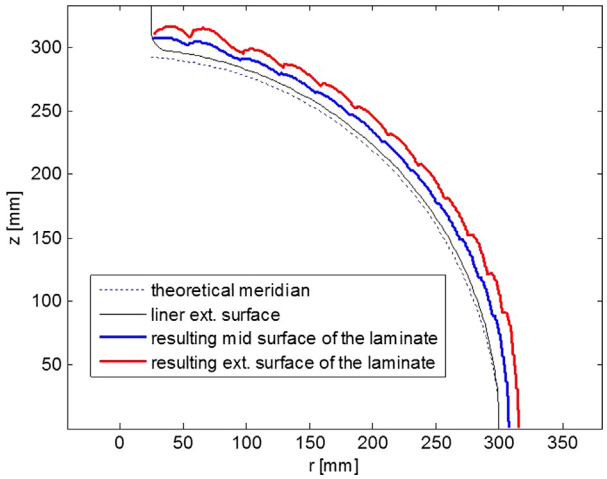

Fig. 4. Laminate thickness distribution in a spherical COPV.

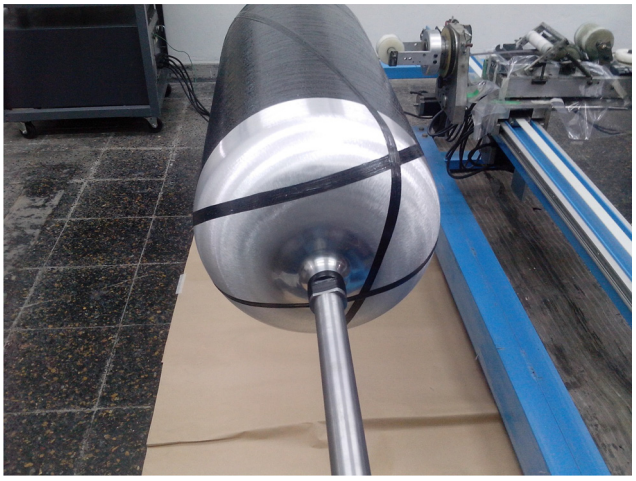

Fig. 5. Winding of a cylindrical COPV.

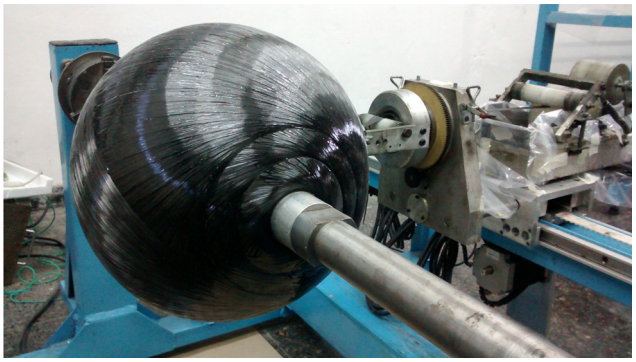

Fig. 6. Winding of a spherical COPV.

3. Modeling the fibers reinforcement mechanical behavior

As mentioned in the Introduction we used two material models, a standard macromechanical material model and a new micromechanical material model, to analyze the mechanical behavior of the COPVs fibers reinforcement.

3.1. The macromechanical model

In this model the composed behavior of the different reinforcement plies is simulated using an orthotropic elastic model with mechanical properties that average the fibers and matrix mechanical properties [6].

This model cannot introduce into the mechanical simulation the matrix cracking; which, as reported in [1] and also observed in the results of our numerical models, has a no negligible effect on the structural behavior of the COPVs. Also, in linerless COPVs, the matrix provides the required sealability and, therefore, it is necessary to predict quite accurately the matrix cracking which is the limiting factor of the COPVs ability to resist internal pressure.

3.2. The micromechanical model

This model introduces for each ply two components,

- an elastic orthotropic layer that simulates the fibers behavior;
- an anisotropic plastic layer (Hill plasticity criterion [7]) that simulates the matrix behavior, incorporating a description of its cracking.

Following [1] let us consider a simple material with only 2 layers: layer (1) representing the fibers and layer (2) representing the matrix.

In what follows we call *dir-1* the fibers direction and *dir-2* the other direction that defines the layers plane. Since the fibers orientation is normally not constant our ad hoc pre-processor defines for each element dir-1, dir-2 and dir-3.

The two layers are assembled using the same shell element nodes (parallel assembly); hence, they are both under the same deformation.

3.2.1. Fibers elastic behavior

Using Voigt notation, for an elastic orthotropic layer, we write Hooke's law as,

$$\boldsymbol{\sigma} = \boldsymbol{C}\ \boldsymbol{\varepsilon}. \tag{6}$$

where

$$\boldsymbol{\sigma} = [\sigma_{11}\ \ \sigma_{22}\ \ \sigma_{33}\ \ \sigma_{12}\ \ \sigma_{23}\ \ \sigma_{31}]^T,$$

$$\boldsymbol{\varepsilon} = [\varepsilon_{11}\ \ \varepsilon_{22}\ \ \varepsilon_{33}\ \ 2\varepsilon_{12}\ \ 2\varepsilon_{23}\ \ 2\varepsilon_{31}]^T.$$

The elastic compliance matrix, $\boldsymbol{C}^{-1}$, is [6],

$$\boldsymbol{C}^{-1} = \begin{bmatrix} \frac{1}{E_1} & \frac{-\upsilon_{12}}{E_2} & \frac{-\upsilon_{13}}{E_3} & 0 & 0 & 0 \\ \frac{-\upsilon_{21}}{E_1} & \frac{1}{E_2} & \frac{-\upsilon_{23}}{E_3} & 0 & 0 & 0 \\ \frac{-\upsilon_{31}}{E_1} & \frac{-\upsilon_{32}}{E_2} & \frac{1}{E_3} & 0 & 0 & 0 \\ 0 & 0 & 0 & \frac{1}{G_{12}} & 0 & 0 \\ 0 & 0 & 0 & 0 & \frac{1}{G_{23}} & 0 \\ 0 & 0 & 0 & 0 & 0 & \frac{1}{G_{31}} \end{bmatrix}. \tag{7}$$

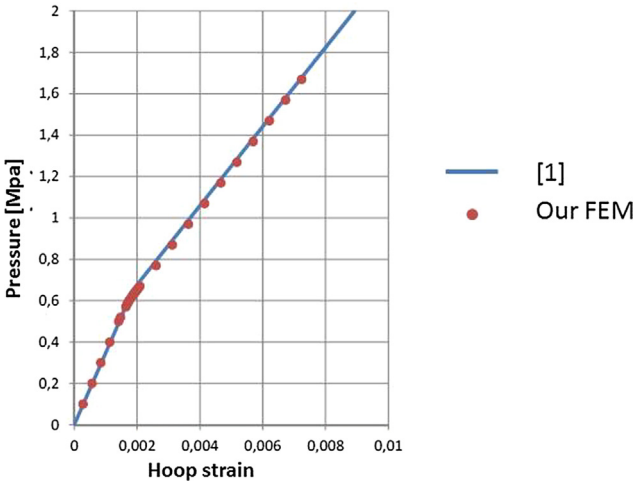

Fig. 7. Structural effect of the matrix fracture.

In the above,

- E_1, E_2, E_3: Young's moduli in *dir-1*, *dir-2* and *dir-3* respectively.
- υ_{ij}: Poisson's ratio for transverse strain in the *dir-i* when stressed in the *dir-j*; that is, $\upsilon_{ij} = \frac{-\varepsilon_{ii}}{\varepsilon_{jj}}$.
- G_{12}, G_{23}, G_{31}: shear moduli in the *1–2, 2–3 and 3–1* planes respectively.

In the orthotropic material there are a total of 9 independent constants and it can be easily shown that $\frac{\upsilon_{ji}}{E_i} = \frac{\upsilon_{ij}}{E_j}$ [6].

There are a number of restrictions for the elastic orthotropic material constants that are properly discussed in [6].

Considering the two layers: fibers layer and matrix layer that simulate the behavior of a composed ply we can write,

$$\boldsymbol{\sigma}^1 = \boldsymbol{C}^1 \ \boldsymbol{\varepsilon}, \tag{8.a}$$

$$\boldsymbol{\sigma}^2 = \boldsymbol{C}^2 \ \boldsymbol{\varepsilon}. \tag{8.b}$$

The stress resultants are,

$$\mathbf{N} = \boldsymbol{\sigma}^1 h_1 a + \boldsymbol{\sigma}^2 h_2 a. \tag{9}$$

In Eq. (9) h_1 and h_2 are the thickness of each layer and a is the layers width. For the equivalent layer we define an equivalent stress tensor $\bar{\boldsymbol{\sigma}}$; hence,

$$\boldsymbol{N} = \bar{\boldsymbol{\sigma}}\,(h_1 + h_2)a \tag{10}$$

Therefore,

$$\bar{\boldsymbol{\sigma}} = \left[\frac{h_1}{h_1+h_2}\boldsymbol{C}^1 + \frac{h_2}{h_1+h_2}\boldsymbol{C}^2\right]\boldsymbol{\varepsilon}. \tag{11}$$

The above term between brackets is the equivalent constitutive matrix ($\boldsymbol{C}^{eq}$).

3.2.2. Matrix plastic behavior

Using an elasto-plastic model we simulate the loss in stiffness induced by the matrix cracking [1]; for this purpose we use the Hill anisotropic yield criterion [7] and an associated flow rule [8].

Since in *dir-1* the loads are mostly carried by the fibers, the matrix cracking can be considered to be triggered when,

$$\left(\frac{\bar{\sigma}_{22}}{\sigma^y_{22}}\right)^2 + \left(\frac{\bar{\sigma}_{12}}{\sigma^y_{12}}\right)^2 = 1. \tag{12}$$

In Eq. (12) σ^y_{22} and σ^y_{12} are material properties and their meaning is evident from that equation.

From Eq. (8),

$$\boldsymbol{\sigma}^1 = \boldsymbol{C}^1 \ \left(\boldsymbol{C}^2\right)^{-1} \ \boldsymbol{\sigma}^2. \tag{13}$$

Replacing in (11) we get,

$$\bar{\boldsymbol{\sigma}} = \left[\frac{h_1}{h_1+h_2}\boldsymbol{C}^1\left(\boldsymbol{C}^2\right)^{-1} + \frac{h_2}{h_1+h_2}\right]\boldsymbol{\sigma}^2. \tag{14}$$

Taking into account that as stated above we are dealing with a plane stress ply and that the constitutive tensors of both layers are collinear,

$$\bar{\sigma}_{22} = \frac{h_1}{h_1+h_2}\left(C^1_{12}S^2_{11} + C^1_{22}S^2_{12}\right)\sigma^2_{11} + \left[\frac{h_1}{h_1+h_2}\left(C^1_{12}S^2_{12} + C^1_{22}S^2_{22}\right) + \frac{h_2}{h_1+h_2}\right]\sigma^2_{22}. \tag{15}$$

In the above equation, $\boldsymbol{S}^2 = \left(\boldsymbol{C}^2\right)^{-1}$.

In Fig. 7 we display the result obtained when modeling a cylinder under internal pressure with three plies (36°, −36°, 90°). It can be observed in the load-displacement curve the kink indicating the matrix fracturing.

Fig. 8. Split disk sample.

Fig. 9. Split ring test assembly.

Table 1
Split disk tests.

Batch	Winding angle	% fibers in volume	% Super position	Fibers equivalent σ_{ult} [MPa]	Average ultimate tensile load [N]
1 = 2	88.38°	69	0	3,381	74,284
3	89.51°	74	20	3,626	99,529
4	88.38°	80	0	3,920	71,953
5	88.38°	62	0	3,038	85,711

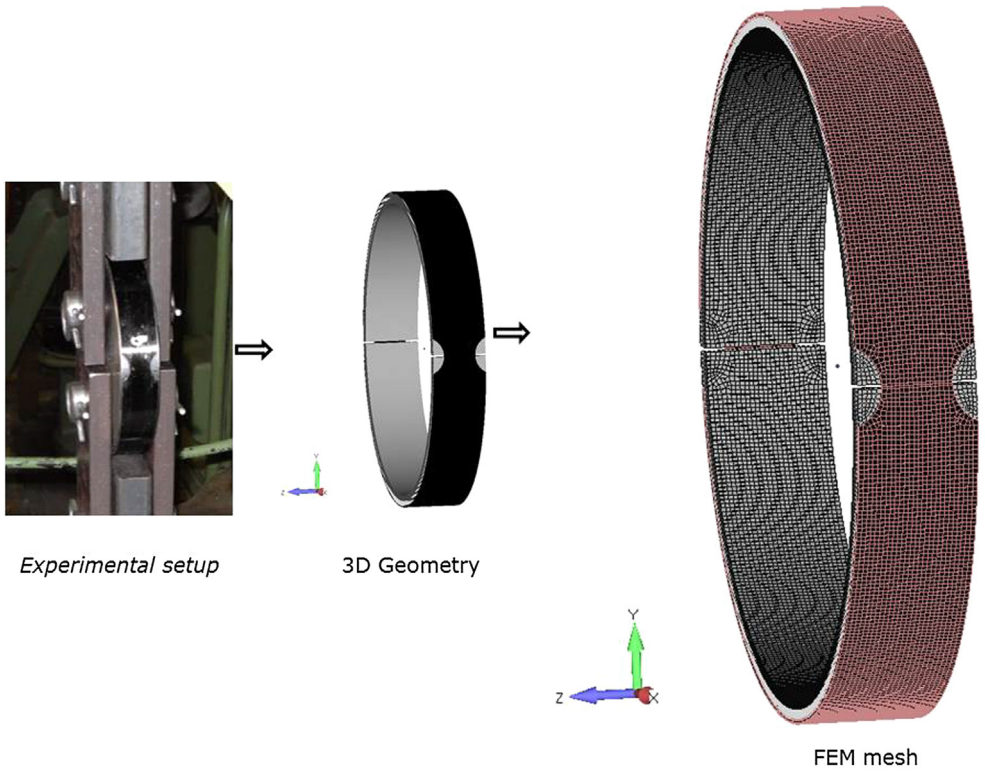

Fig. 10. Split ring model generation.

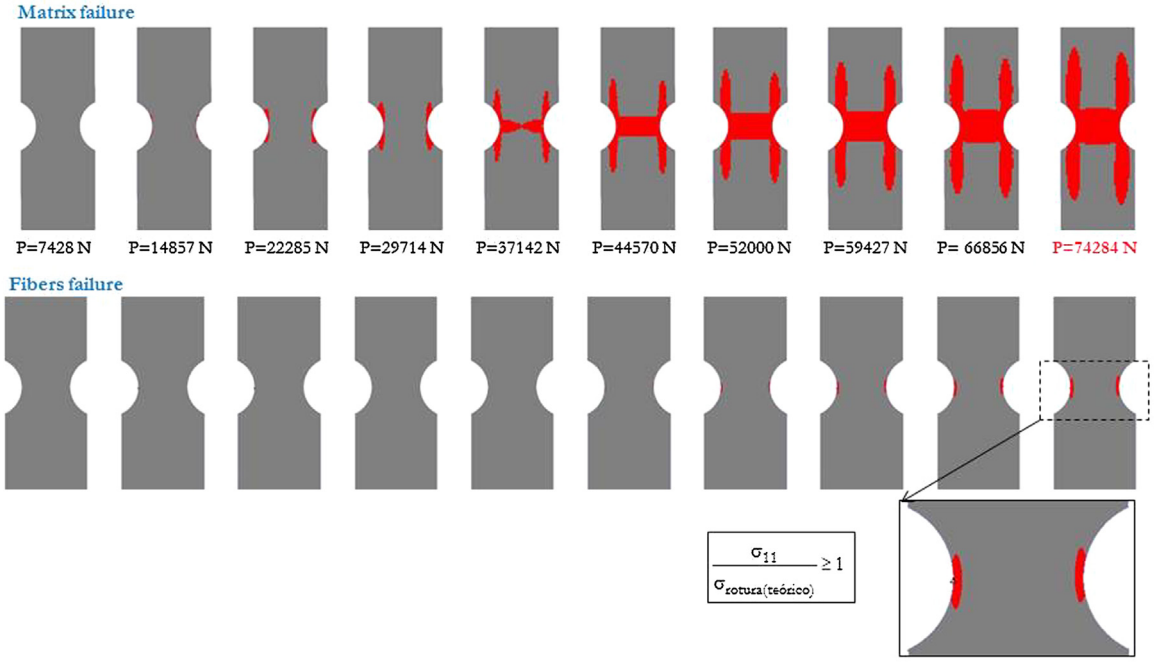

Fig. 11. Failure prediction: macromechanical model.

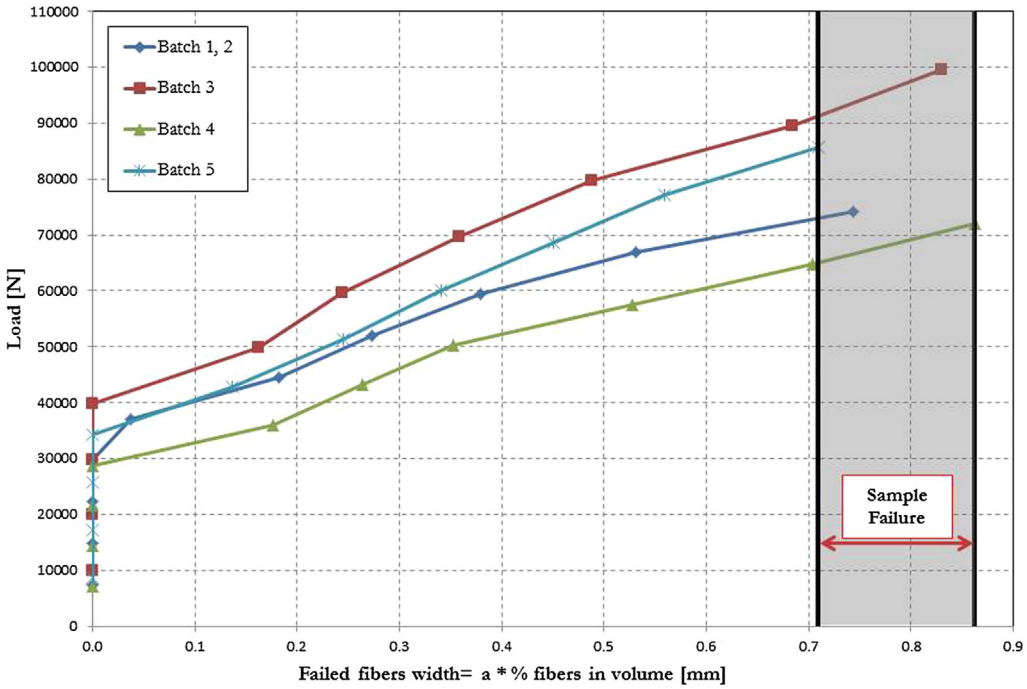

Fig. 12. Determination of the failed fibers with the macromechanical model.

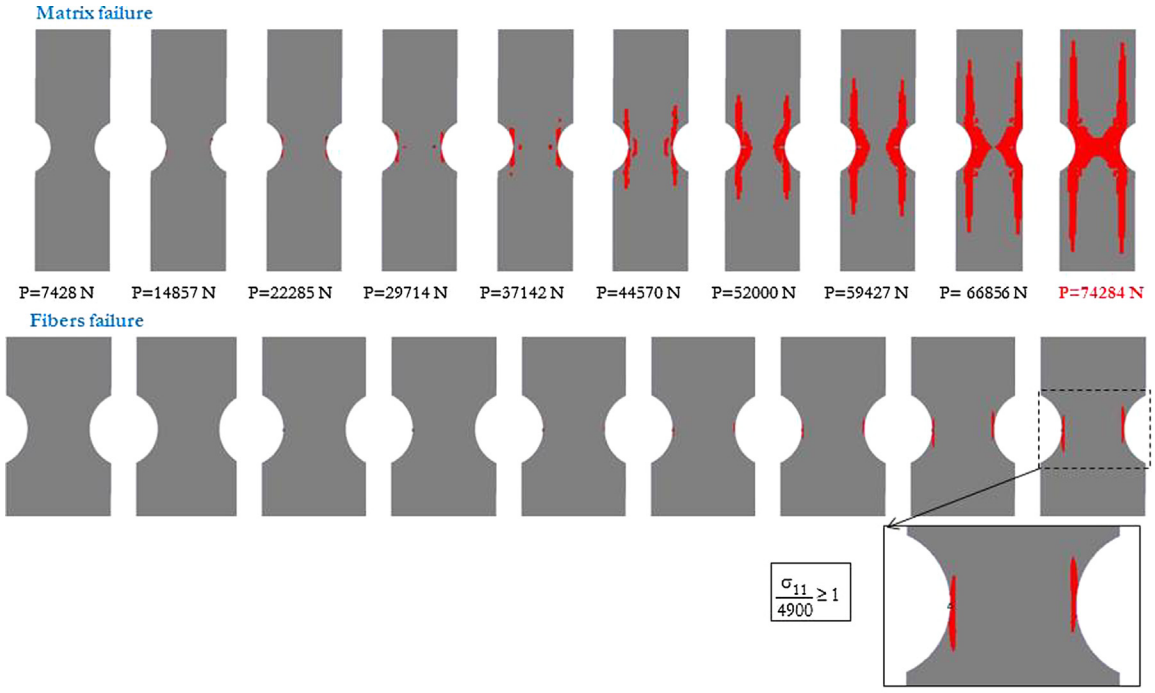

Fig. 13. Failure prediction: micromechanical model.

Much research work is nowadays being developed to include in the numerical simulations the intra-laminar damage [9,10].

4. Computational and experimental results

In this section we discuss two cases,

- a split ring test;
- a cylindrical COPV with ellipsoidal heads under internal pressure.

For both cases we compare the computational results with experimental results.

4.1. The split ring test

The standard test for measuring the strength of a fiber reinforced laminate is the *split disk test* [11].

The samples, shown Fig. 8, are assembled in a tensile machine with a metal split disk that pulls from the samples (Fig. 9).

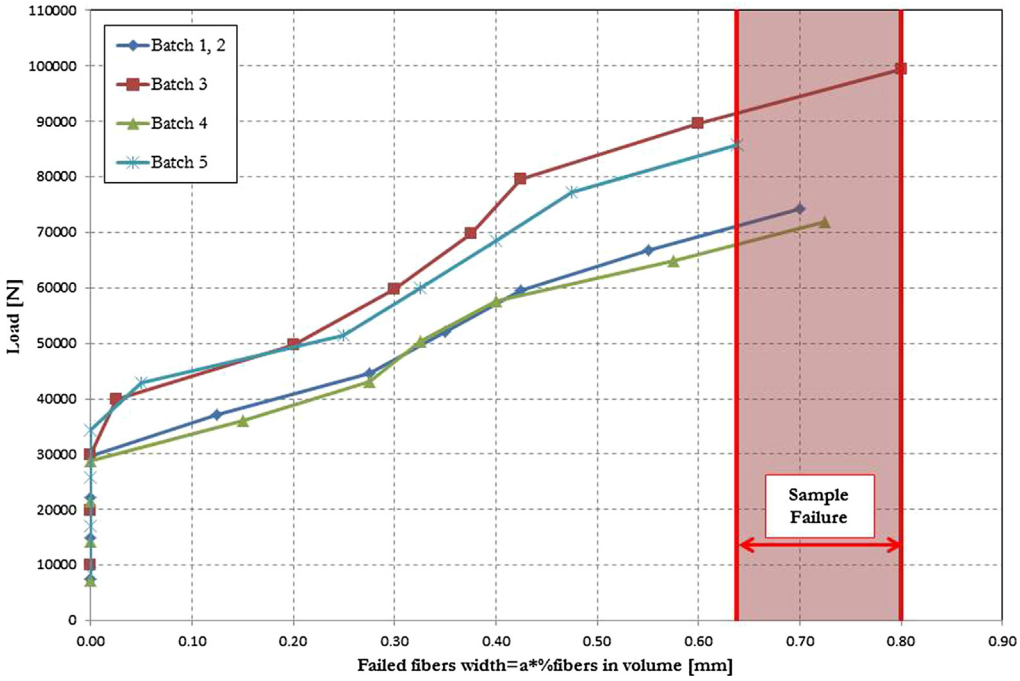

Fig. 14. Determination of the failed fibers with the micromechanical model.

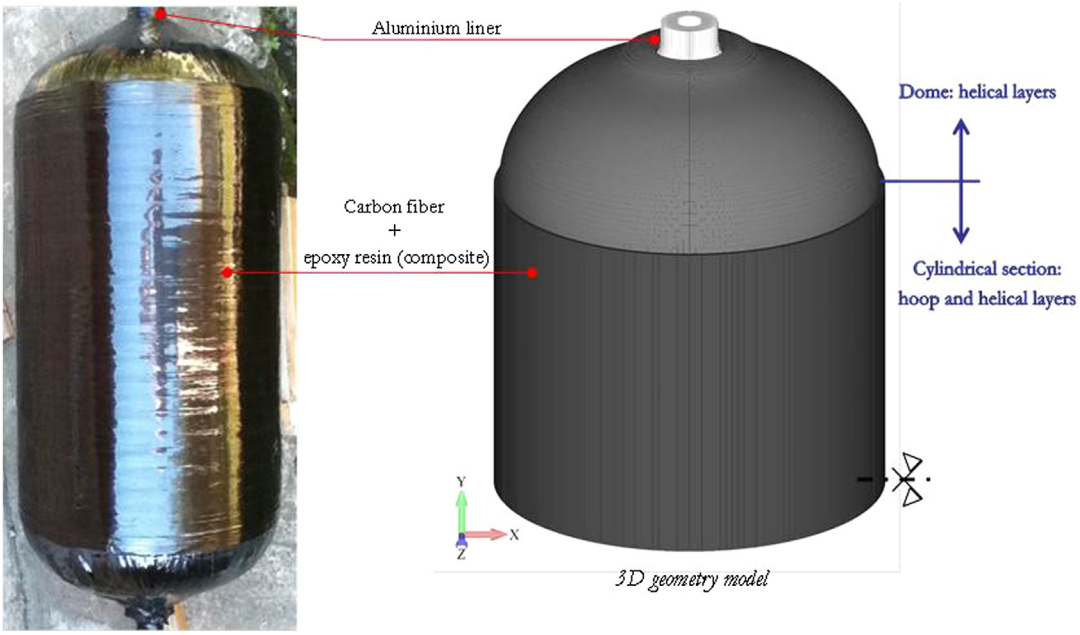

Fig. 15. The 50 lts COPV.

Five batches of samples were constructed as per Table 1; in this table we also present the average ultimate tensile load for each batch.

All the experimental tests were performed at Materials and Structures Lab, Engineering School, University of Buenos Aires[4].

In the above table,

$$\sigma_{ult} = (\%fibers\ \ in\ \ volume)ULT \tag{16}$$

where *ULT* is the tensile strength of the carbon fiber (for the cases under analysis *ULT = 4900 MPa*).

Two finite element models were developed using the MITC4 [5] layered shell element in ADINA [4] to simulate the fibers reinforcement mechanical behavior: one model was developed using the macromechanical model and the other one using the micromechanical model.

To post-process the results we used the Tsai-Hashin failure criterion [4], which indicates that a ply fails if one of the following conditions is fulfilled,

[4] The tests were planned and executed by Germán Kokubu, Ezequiel Poodts and Professor Alejandro Verri.

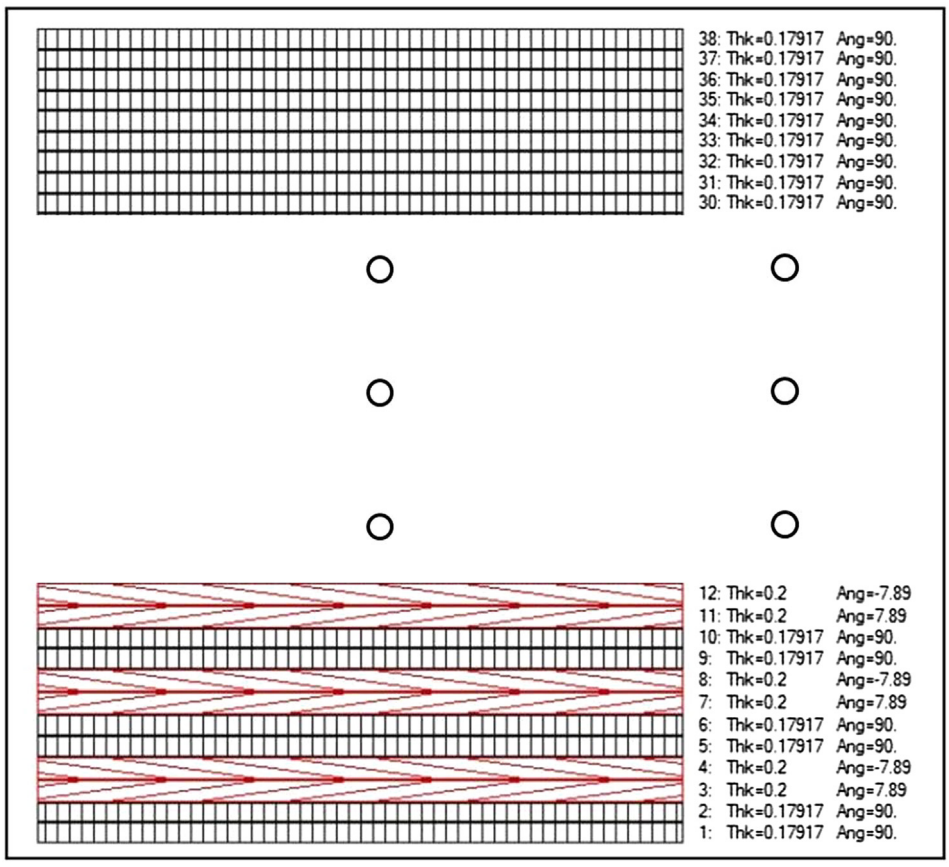

Fig. 16. Laminate configurations for the 50 lts COPV.

$$\frac{\sigma_{11}}{\sigma_{11}^{L+}} \geq 1 \quad (if\ \ \sigma_{11} > 0) \quad Tensile\ \ fibers\ \ failure \tag{17.a}$$

$$\frac{\sigma_{11}}{\sigma_{11}^{L-}} \geq 1 \quad (if\ \ \sigma_{11} < 0) \quad Compressive\ \ fibers\ \ failure \tag{17.b}$$

$$\left(\frac{\sigma_{22}}{\sigma_{22}^{L+}}\right)^2 + \left(\frac{\sigma_{12}}{\sigma_{12}^{L}}\right)^2 \geq 1 \quad (if\ \ \sigma_{22} > 0) \quad Tensile\ \ matrix\ \ failure \tag{17.c}$$

$$\left(\frac{\sigma_{22}}{2\sigma_{23}^{L}}\right)^2 + \left[1 - \left(\frac{\sigma_{22}^{L-}}{2\sigma_{23}^{L}}\right)^2\right]\frac{\sigma_{22}}{\sigma_{22}^{L-}} + \left(\frac{\sigma_{12}}{\sigma_{12}^{L}}\right)^2 \geq 1 \quad (if\ \ \sigma_{22} < 0) \quad Compressive\ \ matrix\ \ failure \tag{17.d}$$

In the above, for each ply, the following properties are defined for each particular combination fibers – matrix,

σ_{11}^{L+}: limit tensile stress in the *1-direction* (fibers direction);
σ_{11}^{L-}: limit compressive stress in the *1-direction* (fibers direction);
σ_{22}^{L+}: limit tensile stress in the *2-direction* (orthogonal to the fibers direction);
σ_{22}^{L-}: limit compressive stress in the *2-direction* (orthogonal to the fibers direction);
σ_{12}^{L}: limit shear stress in the *plane 1–2*;
σ_{23}^{L}: limit shear stress in the *plane 2–3*.

In Fig. 10 we show a scheme of the finite element model which is composed by 32,800 MITC4 layered elements [5 12].

4.1.1. Macromechanical model results

In Fig. 11 we present, for batches 1 and 2 which have an ultimate load off 74,824N, the sample zones where matrix or fibers failure are predicted using the macromechanical model together with the Tsai-Hashin failure criterion.

For the other batches the failure predictions are identical within a few tenths of a millimeter.

Post-processing, for the different batches, the finite element results together with the data in Table 1, we get the curves in Fig. 12 from which we can determine the maximum amount of

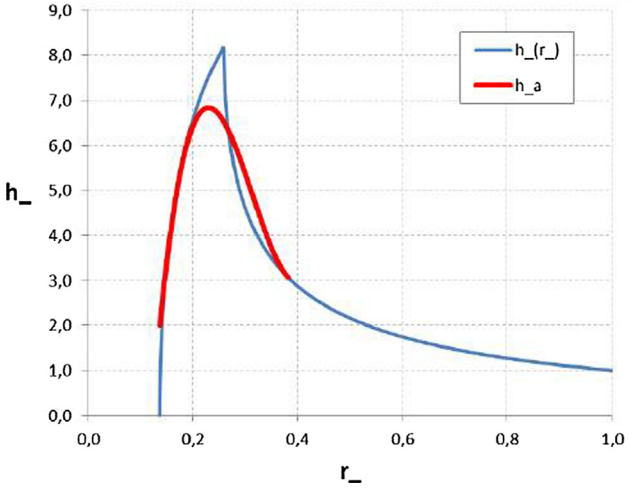

Fig. 17. Thickness distributions for the 50 lts COPV.

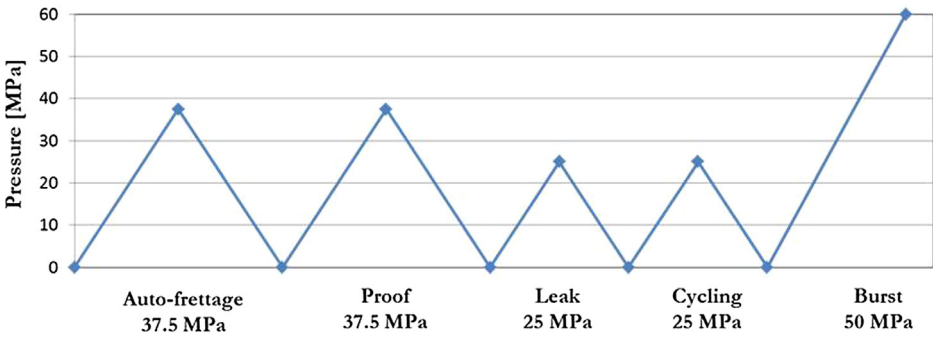

Fig. 18. Pressure cycle.

Table 2
6061-T6 aluminum liner.

E [GPa]	ν	σ_y [MPa]	ε_u [%]	σ_u [MPa]
68.9	0.33	242	11.5	310

Table 3
Laminate mechanical properties.

Model	Material	E1 [MPa]	E2 [MPa]	G [MPa]
Macromechanical	Laminae	103,500	10,000	5,000
Micromechanical	Fibers	230,000	0	0
	Matrix	230	4,327	11,111

fibers that can fail without implying a complete failure of the sample. It is important to notice that it is not enough to have a minimum amount of fibers failure to have a structural failure.

4.1.2. Micromechanical model results

In Figs. 13 and 14 we again present the results obtained analyzing the split ring tests listed in Table 1; but this time we performed the numerical analyzes using the micromechanical material model.

Comparing Fig. 12 with Fig. 14 is quite obvious that for the split ring test both material models provide results that for practical purposes are coincident.

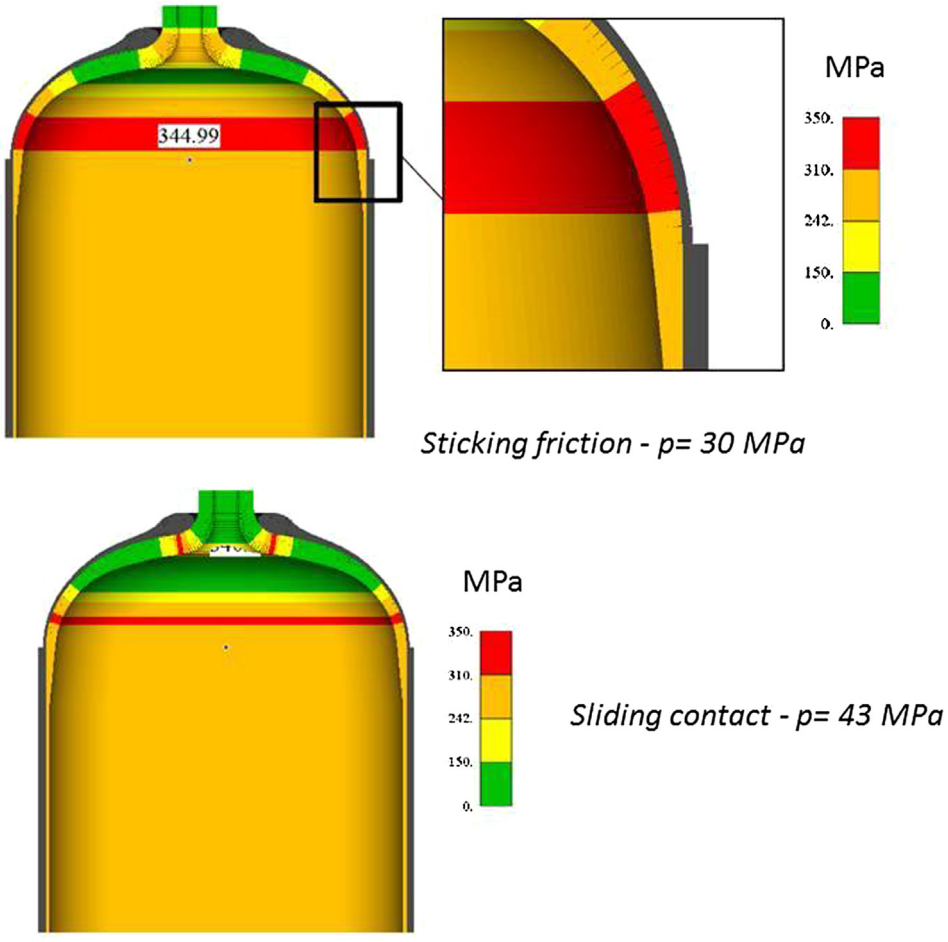

Fig. 19. Macromechanical model. Principal stresses predicted in the liner.

Table 4
Failure pressures predicted using the micromechanical model.

	Liner	Sticking friction 60 MPa	Sliding contact 43 MPa
Cylindrical section	1st circumferential layer	52 MPa	48 MPa
	1st helicoidal layer	52 MPa	42 MPa
Ellipsoidal head	1st helicoidal layer	55 MPa	25 MPa

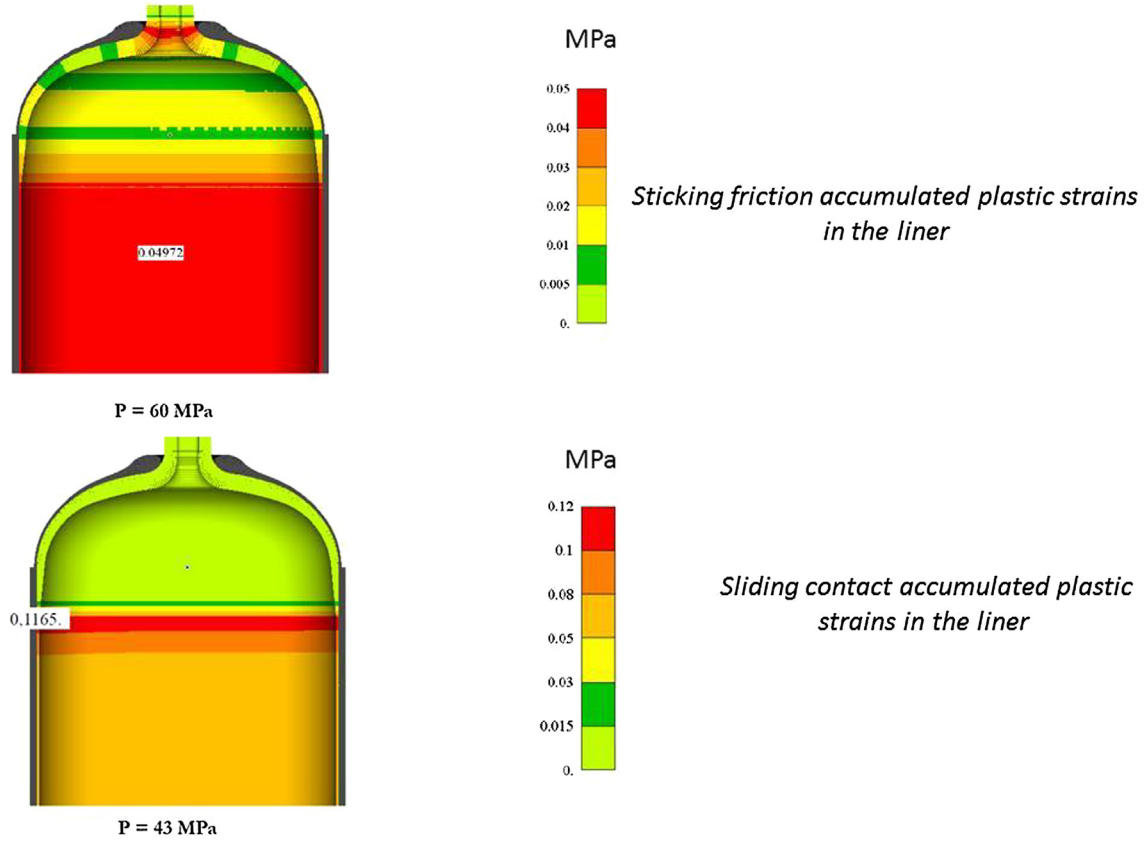

Fig. 20. Failure due to plastic deformation in the liner.

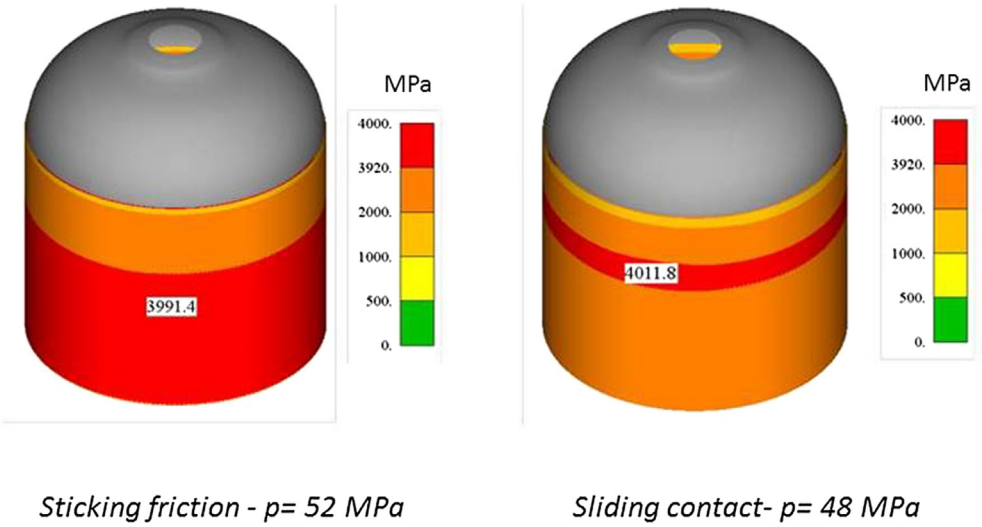

Fig. 21. Stresses in the first circumferential layer of the cylindrical section.

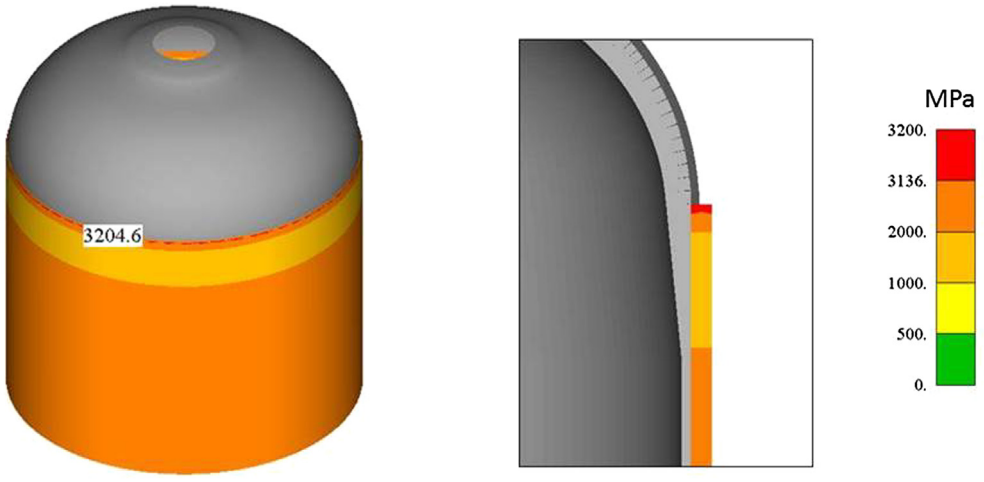

Fig. 22. Stresses in the first helicoidal layer of the cylindrical section.

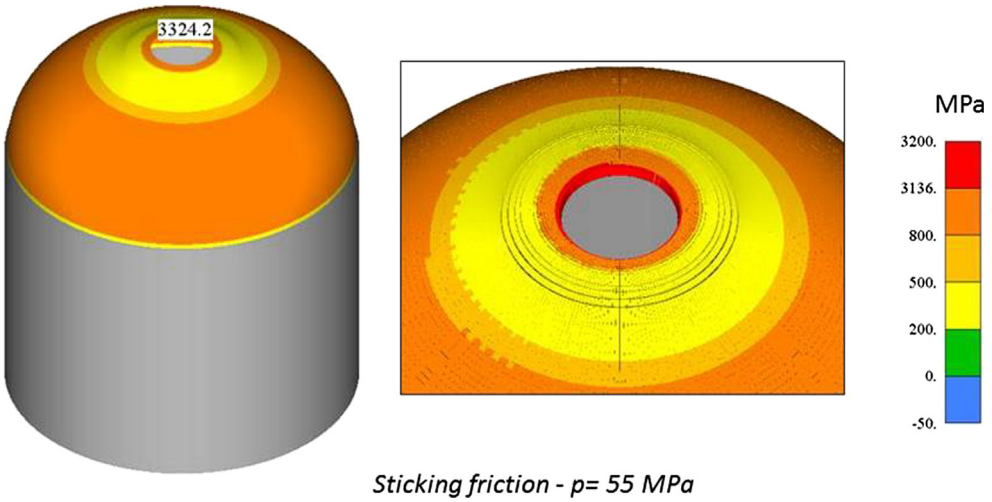

Fig. 23. Stresses in the first helicoidal layer of the ellipsoidal head (sticking friction).

4.2. Cylindrical COPV with ellipsoidal heads under internal pressure

In Fig. 15 we present a sketch of a 50 lts COPV.

We describe its modeling and experimental test in the present sub-section.

The laminate configuration is indicated in Fig. 16 and the resulting thickness distribution in Fig. 17. The percentage of fibers in the volume was 45%.

We compare the results with experimental results aiming at a cross validation,

- validation of the numerical results: when the numerical results match the experimental determinations, as usual, we validate the numerical model;
- validation of the manufacturing procedures: when the experimental determinations match the numerical results we can assess that the manufactured COPV works as planned in the design and therefore the manufacturing procedures produced a product within the specified features.

The design of this COPV has to fulfil,

- Maximum Expected Operating Pressure (MEOP): 25 MPa;
- Proof Pressure (auto-frettage): 37.5 MPa;
- Minimum Burst Pressure 50 MPa.

Following [2] the test cycle in Fig. 18 was established.

Only one cycle was modeled because the computational results indicate that no increase in the liner accumulated plastic deformation is observed during the cycling (shake down behavior).

The strength limit of the vessel is reached when either the fibers reach its ultimate tensile strength or when the equivalent plastic strain in the liner reaches at any point its ultimate strain.

4.2.1. The finite element model

Two finite element models were developed, one using the macromechanical model for the laminate material and the other one using the micromechanical model.

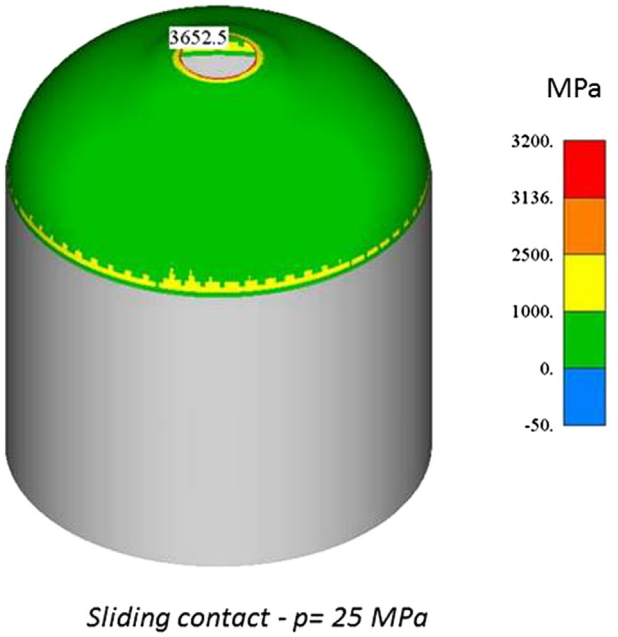

Fig. 24. Stresses in the first helicoidal layer of the ellipsoidal head (sliding contact).

For both cases,

- the liner was modeled using MITC4 shell elements together 3D 8-node elements for the end-bosses;
- the laminate was modeled using layered MITC4 elements;
- the two models included a contact condition between the laminate material and the liner. In order to account for the uncertainty on the friction coefficient two cases were considered for each model: sticking friction and sliding friction.

The mechanical properties of the aluminum liner (6061-T6) [13] are shown in Table 2 and the mechanical properties considered for both material models are listed in Table 3.

The ultimate stresses for laminate are,

$$\sigma_u^{90^\circ} = 0.8 \cdot \%vol_{fibers} \cdot \sigma_u^{fibers},$$

$$\sigma_u^{\varphi} = 0.8 \cdot 0.8 \cdot \%vol_{fibers} \cdot \sigma_u^{fibers}.$$

The factors – *0.8* – are specified in [1] to take into account the deterioration of the fibers during the manufacturing process.

4.2.2. Macromechanical model: finite element results

In Fig. 19 we show the principal stresses predicted by the finite element model. It can be seen that for the sticking friction assumption the ultimate liner stress is reached for an internal pressure of 30 MPa while for the sliding contact assumption the ultimate liner stress is reached for an internal pressure of 43 MPa.

The macromechanical model overestimates the peak stresses induced by the shape of the vessel; the overestimation comes from the fact that the laminate behavior is simulated using a pure elastic model.

Hence, we decided to exclusively use the micromechanical model to evaluate the COPVs mechanical strength. The agreement between the micromechanical model predictions and the experimental results, to be discussed in the next sub-section, confirmed the validity of our decision.

4.2.3. Micromechanical model: finite element results

In Table 4 we indicate the pressures that produce failure in the liner and in the laminate.

For the sticking friction condition the liner can reach an internal pressure of 60 MPa without failure and for the frictionless condition the liner reaches the maximum plastic deformation that the aluminum can undergo for an internal pressure of 43 MPa (Fig. 20)

In Figs. 21–23 we present some typical stress distributions in the laminates.

Even though for the condition of sliding contact the maximum allowable stress at the first helicoidal layer of the laminate is reached at only 25 MPa (see Table 4) the material volume affected by those stress is very limited and therefore it is not considered an indication of the vessel failure (see Fig. 24).

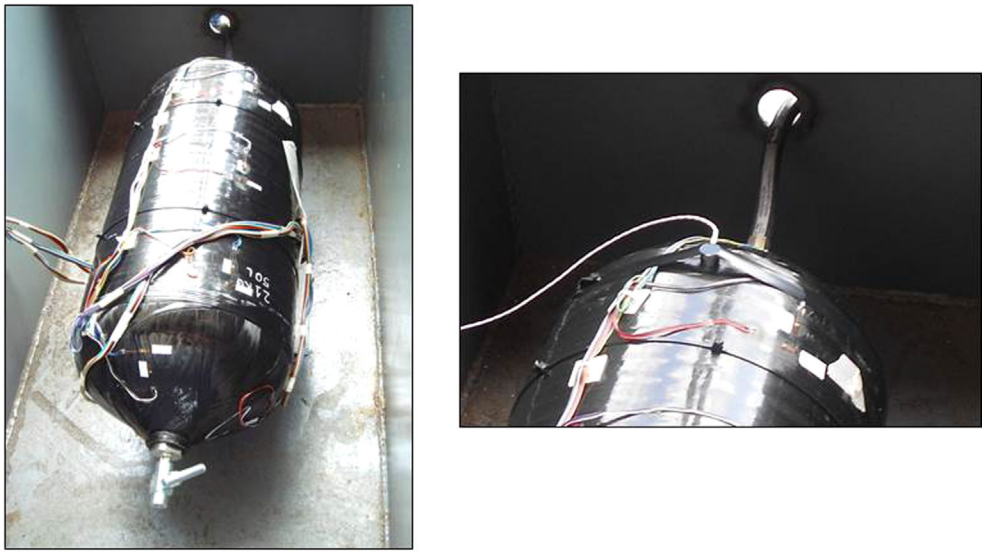

Fig. 25. Instrumented COPV.

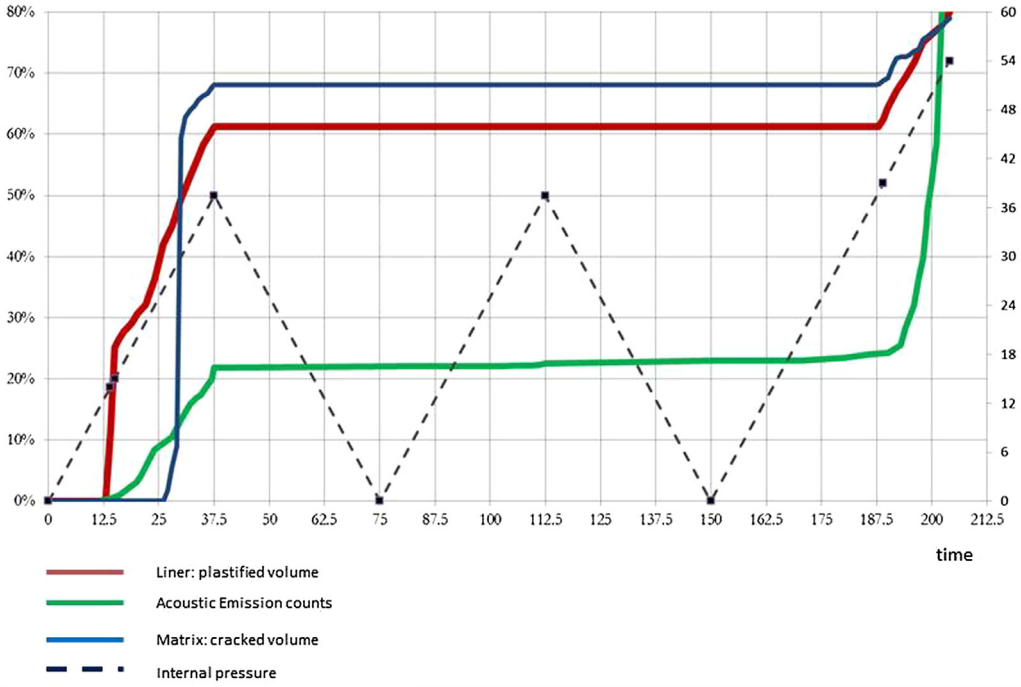

Fig. 26. Acoustic emission.

4.2.4. Experimental validation of the finite element results

A COPV was tested with the pressure cycle in Fig. 18. In Fig. 25 we show the testing set up, which was instrumented with strain gages and microphones to detect acoustic emissions[5].

The measured burst pressure was 54 MPa while the finite element predicted burst pressure was 52 MPa (sticking friction condition); hence, $p^{burst}_{FEM}/p^{burst}_{experimental} = 0.96$.

It is very interesting to observe the agreement between the acoustic emission output and the numerical results. In Fig. 26 the "*counts*" of the acoustic emission test are compared with the finite element results for the liner plastic volume and for the matrix cracked volume, it is evident that the three results show the same qualitative behavior.

5. Conclusions

The finite element results and experimental results shown in this paper indicate that the modeling of COPVs should be developed incorporating into the model,

- the liner (metallic) elasto-plastic behavior,
- the fibers elastic orthotropic behavior,
- the matrix plastic anisotropic behavior to model the matrix cracking.

It was shown that micromechanical material model of the fibers reinforcement, developed in this paper, is a reliable finite element procedure for the calculation and design of COPVs.

Finally, another important conclusion is that the acoustic emission test can be used as a very valuable tool for extracting as much information as possible from the COPVs qualifications tests.

[5] The acoustic emission detection was carried out by the CNEA (National Atomic Energy Commission).

Acknowledgements

We acknowledge the development and leadership of the COPV technological project to VENGSA, one of the main aerospace companies of Argentina (http://www.veng.com.ar/); and the excellent winding of the prototypes by Kohlenia, an Argentinian technological small industry specialized in carbon fiber parts (http://www.kohlenia.com/).

References

[1] Vasiliev VV. Composite pressure vessels: analysis, design and manufacturing. Bull Ridge Corporation; 2009.
[2] AIAA. Space systems – composite overwrapped pressure vessels (COPVs) (S-081A-2006); 2006.
[3] ECSS. Space Engineering. Structural design and verification of pressurized hardware (ECSS-ST-32-02C Rev.1); 2008.
[4] ADINA R&D. ADINA users manual. Watertown, MA, USA; 2012.
[5] Dvorkin E, Bathe K-J. A continuum mechanics based four-node shell element for general nonlinear analysis. Eng Comput 1984;1(1):77–88.
[6] Jones RM. Mechanics of composite materials. Washington, D.C.: McGraw Hill; 1975.
[7] Hill R. The mathematical theory of plasticity. Oxford University Press; 1983.
[8] Dvorkin E, Goldschmit M. Nonlinear continua. Springer; 2005.
[9] Riccio A, Sellitto A, Saputo S, Russo A, Zarrelli M, Lopresto V. Modelling the damage evolution in notched omega stiffened composite panels under compression. Compos B Eng 2017;126:60–71.
[10] Sellitto A, Riccio A, Russo A, Zarrelli M, Toscano C, Lopresto V. Compressive behaviour of a damaged omega stiffened panel: Damage detection and numerical analysis. Compos Struct 2019;209:300–16.
[11] ASTM D 2290. Standard test method for apparent hoop tensile strength of plastic or reinforced plastic pipe by split disk method; 2003.
[12] Bathe K-J. Finite element procedures. Prentice Hall; 1996.
[13] Metals Handbook. ASM.